applied sciences

MDPI

Article

Research on a Novel Nanosecond Marx Generator and Its Efficiency Analysis

Zi Li [1], Yuan Chai [1], Song Jiang [1] and Junfeng Rao [2,*]

[1] Department of Electrical Engineering, University of Shanghai for Science and Technology, No. 516 Jungong Road, Shanghai 200093, China
[2] Suzhou Institute of Biomedical Engineering and Technology, Chinese Academy of Sciences, Suzhou 215163, China
* Correspondence: raojf@sibet.acn.cn

Abstract: The traditional Marx generators based on avalanche BJTs usually use a DC voltage source to charge the storage capacitors, and many theoretical studies have proved that the existence of DC voltage source leads to low energy efficiency. This paper proposes a novel nanosecond Marx generator based on avalanche BJTs, which is charged by a series-resonant power supply. This power supply charges all capacitors with a constant average current and all BJTs avalanche breakdown stage by stage without any triggering signals. When the resistors are replaced by inductors, the efficiency can be further improved. The pulse repetition frequency can be adjusted by controlling the resonant average current. The output voltage can be increased by connecting more avalanche BJTs in series or increasing the number of stages of the Marx generators. The control method and the structure of the circuit are simple. Experimental results show that negative pulses with an adjustable frequency of 10–60 kHz, a pulse width of 8.45 ns, and an amplitude of 4 kV were obtained on a resistive load. The energy efficiency of the Marx generator was increased to 94%.

Keywords: nanosecond pulse; Marx generator; energy efficiency; avalanche BJT

Citation: Li, Z.; Chai, Y.; Jiang, S.; Rao, J. Research on a Novel Nanosecond Marx Generator and Its Efficiency Analysis. *Appl. Sci.* **2022**, *12*, 9800. https://doi.org/10.3390/app12199800

Academic Editor: Andreas Sumper

Received: 13 May 2022
Accepted: 5 June 2022
Published: 29 September 2022

1. Introduction

Nanosecond Marx generators are widely used in many fields, such as material processing, biomedical engineering, high power microwave technology, and so on [1–3]. Fast semiconductor switches, such as insulated gate bipolar transistors (IGBTs), Metal-Oxide-Semiconductor field-effect transistors (MOSFETs), and bipolar junction transistors (BJTs) [4,5], are the key components in these Marx generators. However, the switching speeds of IGBT and MOSFET decrease with the increase in the conduction current, then the front edges of output pulses are limited. A nanosecond conduction velocity could be obtained if the Collector and Emitter of the BJTs avalanche break down [6,7]. Therefore, avalanche BJTs are often used to generate nanosecond high-voltage pulses in Marx generators. To obtain high-frequency nanosecond pulses with fast rising and falling edges, T. Pi et al. [8] improved the traditional Marx generator based on the avalanche BJTs and increased the charging speed. An output pulse with 1.08 kV and 50 kHz was obtained, and the energy efficiency of the generator was about 26.67%. W. Zhang et al. [9] adopted multiple Marx generators in parallel to increase the output current amplitudes. Nanosecond pulses with a rising time of 3.4 ns, an amplitude of 2.5 kV, and a repetitive frequency of 15 kHz were obtained over a 50 Ω resistor load. The energy efficiency was about 38%. To improve the reliability of high-power Marx generators based on avalanche BJTs, W. Ding et al. [10] developed an auxiliary triggering topology. The output voltage and the rise time were 4 kV and 6 ns over a coaxial cable with 50 Ω impedance. The voltage efficiency was about 37%.

From the research mentioned above, it can be found that the energy efficiency of the generators using avalanche BJTs is low, and the analytical method needs to be improved. So far, all these Marx generators based on avalanche BJTs are charged by DC voltage supplies,

which causes the energy efficiency to be lower than 50% [8,9]. The charging loops are indicated by the blue arrow lines, and the discharging loop is indicated by the red line in Figure 1. This paper proposes a novel nanosecond Marx generator using a series-resonant charging power supply based on the avalanche BJTs. The energy efficiency is analyzed in detail, and an optimization scheme is proposed to improve the energy efficiency. From the experimental results, the charging efficiency of the capacitors and the energy efficiency of this Marx generator have been significantly improved.

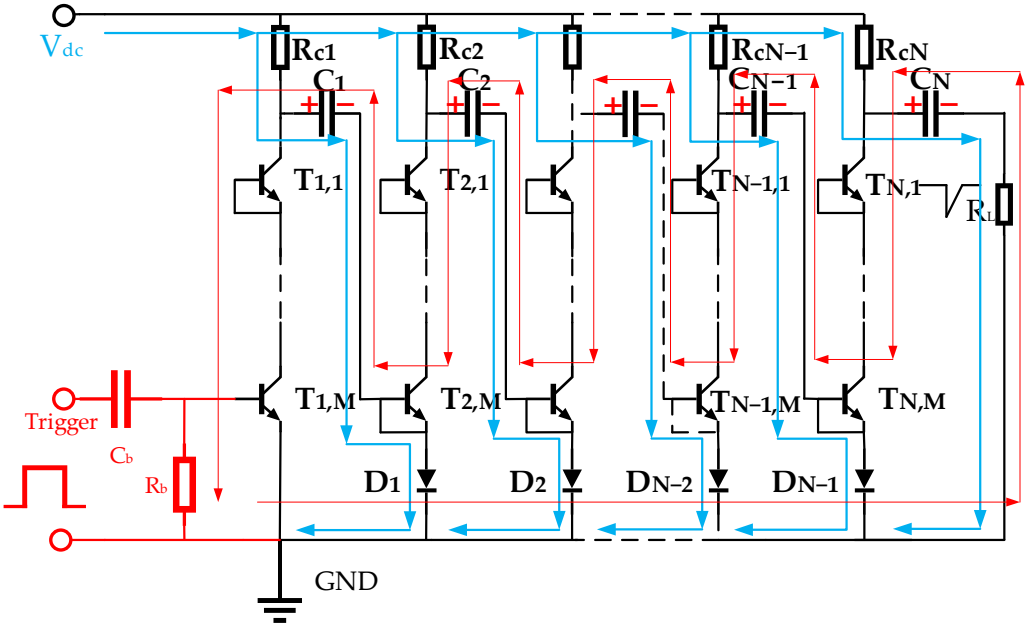

Figure 1. The traditional N × M stage Marx generator based on avalanche BJTs.

2. The Proposed Nanosecond Pulse Generator

The new topology of the nanosecond Marx generator is proposed, as shown in Figure 2. It consists of the series-resonant charging power supply and a 3 × 5 stage Marx generator based on avalanche BJTs.

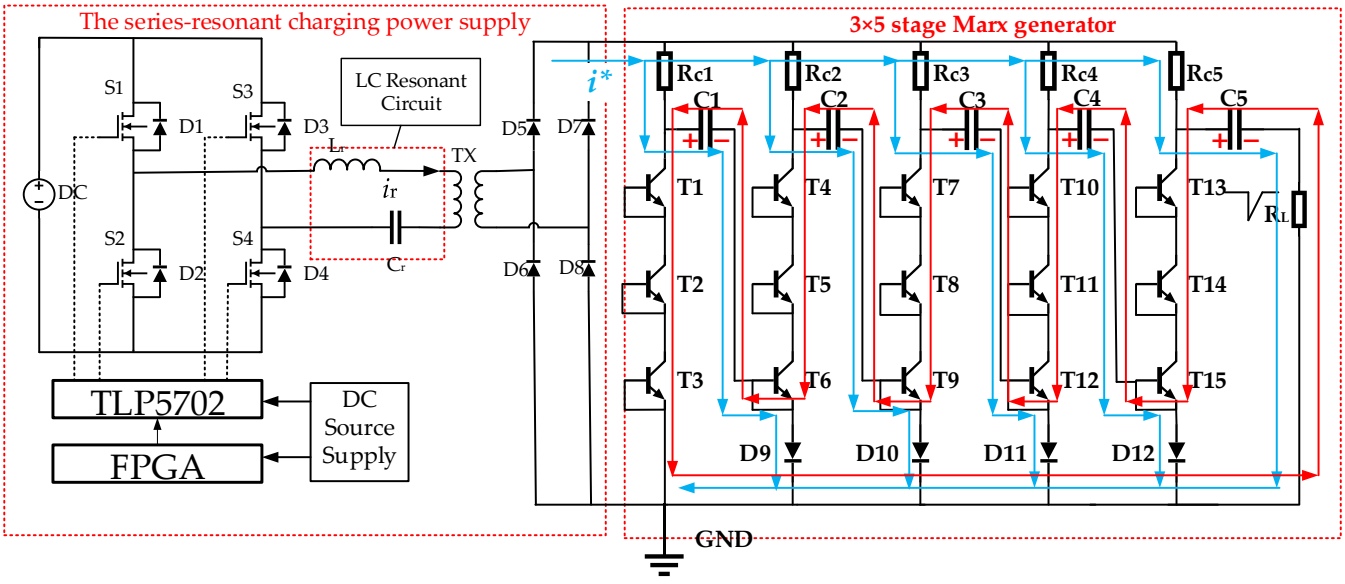

Figure 2. The schematic of the proposed nanosecond Marx generator (circuit I).

2.1. The Series-Resonant Charging Power Supply

Compared with the traditional DC voltage source, the full-bridge series-resonant source has small volume and high-efficiency advantages. L_r is the resonant inductance and C_r is the resonant capacitance. The Field Programmable Gate Array (FPGA) controls the switches S1~S4 through the driver chips TLP5702. The switches S1~S4 are turned on sequentially through timing control and a resonant current i_r is generated. The resonant current passes through the transformer to charge the energy-storage capacitors $C_{1\sim5}$.

According to the relationship between the full-bridge switching frequency f_s and the resonant frequency f_r, the circuit can work in three modes [11,12], one discontinuous current mode (DCM, where $f_s < 0.5f_r$) and two continuous current modes (CCM, where $0.5f_r < f_s < f_r$ or $f_s > f_r$). In the DCM mode, the switches can realize zero-current turn-on and turn-off and reduce the switching loss. Therefore, the discontinuous current mode was chosen in this research. The waveform diagram of the main operating points of the series resonant capacitor charging circuit in DCM is shown in Figure 3 [13]. C' is the equivalent capacitance of the energy-storage capacitor $C_{1\sim5}$. It can be seen that the voltage on the energy-storage capacitor increases evenly.

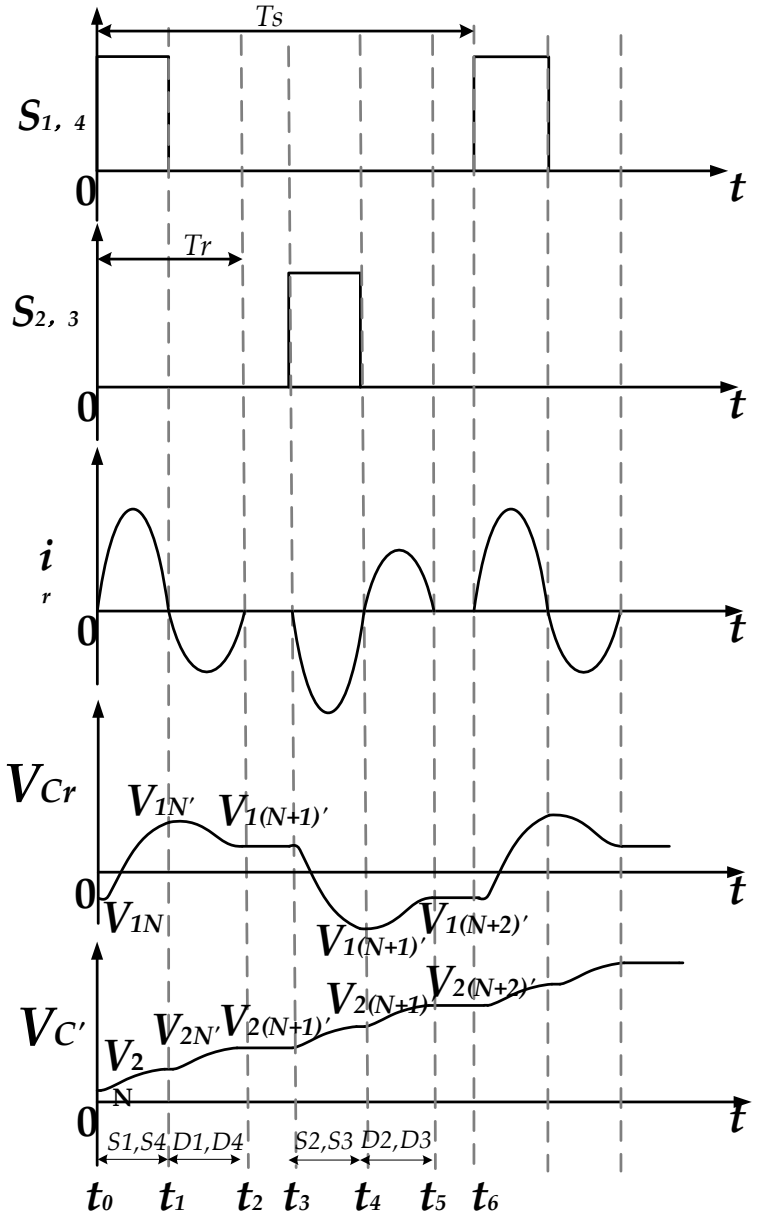

Figure 3. The waveform of series resonant circuit in DCM.

Within a switching cycle T_s, the operation of the series-resonant charging source can be divided into four phases [13,14]. In phase 1, the switches S1 and S4 are turned on, and the DC source charges C_r through L_r, $i_r > 0$. In phase 2, the switches S1 and S4 are turned off, and C_r charges L_r through continuous diodes D1 and D4, $i_r < 0$. Phase 3 is the same as phase 1, except that the switches S2 and S3 are turned on, $i_r < 0$. Phase 4 is the same as phase 2, except that C_r charges L_r through continuous diode D2 and D4, $i_r > 0$.

The resonant current I(t) can be derived during the charging period, as shown in Equation (1). I(t) represents the resonant current in a switching cycle. At this point, the effect of isolation resistance R_c can be ignored.

$$I(\mathrm{t}) = \begin{cases} \frac{V_{dc}-V_{1N}-V_{2N}}{\omega L_r}\sin\omega(t-t_0), & t_0 < t < t_1 \\ \frac{V_{dc}-V_{1N'}+V_{2N'}}{\omega L_r}\sin\omega(t-t_1), & t_1 < t < t_2 \\ \frac{-V_{dc}-V_{1(N+1)}+V_{2(N+1)}}{\omega L_r}\sin\omega(t-t_3), & t_3 < t < t_4 \\ \frac{-V_{dc}-V_{1(N+1)'}-V_{2(N+1)'}}{\omega L_r}\sin\omega(t-t_4), & t_4 < t < t_5 \\ 0, & t_2 < t < t_3,\ t_5 < t < t_6 \end{cases} \quad (1)$$

Here,

$$\omega = \sqrt{\frac{1}{L_r C_r} + \frac{1}{L_r C'}} \quad (2)$$

where C' is the equivalent capacitance of the energy-storage capacitor $C_{1\sim5}$, subscript N represents the Nth resonant period, and ω is the angular frequency of the resonant loop.

The average charging current I_{avg}, which is constant in a resonant period T_r, can be expressed by Equation (3). I_{peak} is the peak current of each phase.

$$I_{avg} = \frac{1}{2} \times \frac{2}{\pi}\left(I_{peak1,3} + I_{peak2,4}\right) = \frac{2}{\pi} \times \frac{C' - C_r}{(C' + C_r)\omega L_r} V_{dc} \quad (3)$$

The average charging current I^*_{avg} in a switching period T_s is given by Equation (4) [15]. It can be seen that the average value of resonant current in each cycle is the same and has nothing to do with the number of cycles, which provides a basis for the stabilization of repeated frequency discharge in subsequent experiments.

$$I^*_{avg} = \frac{I_{avg} T_r}{T_s/2} = \frac{8\left(-C_r^2 C' + C_r C'^2\right)}{\left(C_r + C'\right)^2 T_s} V_{dc} \approx \frac{8C_r}{nT_s} V_{dc} \quad (4)$$

where n is the turns ratio of the transformer TX.

When the circuit parameters are determined, the average charging current I^*_{avg} is constant and has nothing to do with the resonant period [15]. Therefore, it can be regarded as a constant current source. However, when the continued current through the reverse parallel diode drops to zero, the average charging current is no longer constant, and the circuit loses its constant current characteristics. At this point, the charging voltage of the capacitor converted to the original site of the transformer is close to the voltage of the pre-stage DC power supply.

The average charging current can be adjusted by changing V_{dc} or switching cycle T_s. Compared with the DC source, the series resonant charging in DCM can realize constant current charging, increasing the voltage of C to avalanche voltage V_{break}. Therefore, the BJTs should break down before it enters the nonlinear charging mode.

2.2. The 3 × 5 Stage Marx Generator Based on Avalanche BJTs

Compared with the traditional Marx generators based on avalanche BJTs, each avalanche BJT in the proposed nanosecond Marx generator turns on through self-breakdown without any triggering signal. The principle of the novel Marx generator is that the capacitors $C_{1\sim5}$ are

charged in parallel by a constant average current as indicated by the blue arrowed lines, and discharge to the load R_L in series as indicated by the red arrowed line in Figure 2.

The series-resonant source charges the capacitors during the charging period, and when the avalanche breakdown voltage V_{break} is reached, it enters the discharge period and automatically discharges to the load. The voltage over the capacitors is related to the number of BJTs in series. When M BJTs are connected in series, the avalanche breakdown voltage is M times the breakdown voltage of a single BJT. Theoretically, the maximum voltage on the storage capacitor is MV_{break}, $V_C = MV_{break}$. In the experiment, MV_{break} is designed to be lower than nV_{dc} so that the series-resonant source always charges the capacitors with a constant current. During the discharging period, the voltage of capacitors is higher than the C-E breakdown voltage of the avalanche BJTs V_{break}, all BJTs avalanche break down, and all diodes are reverse biased. A negative nanosecond pulse is obtained over the load. When the discharge current through the avalanche BJTs is lower than the cutoff current, the BJTs turn off, and the capacitors are charged again in parallel. In this way, repetitive negative pulses are obtained over the load. Pulses with a higher voltage amplitude can be obtained by connecting the number M of avalanche BJTs in series or increasing the number N of stages of the Marx generator. The theoretical waveform of the circuit is shown in Figure 4. The pulse frequency can be adjusted by changing the average charging current. The higher the average charging current is, the higher the pulse repetition frequency.

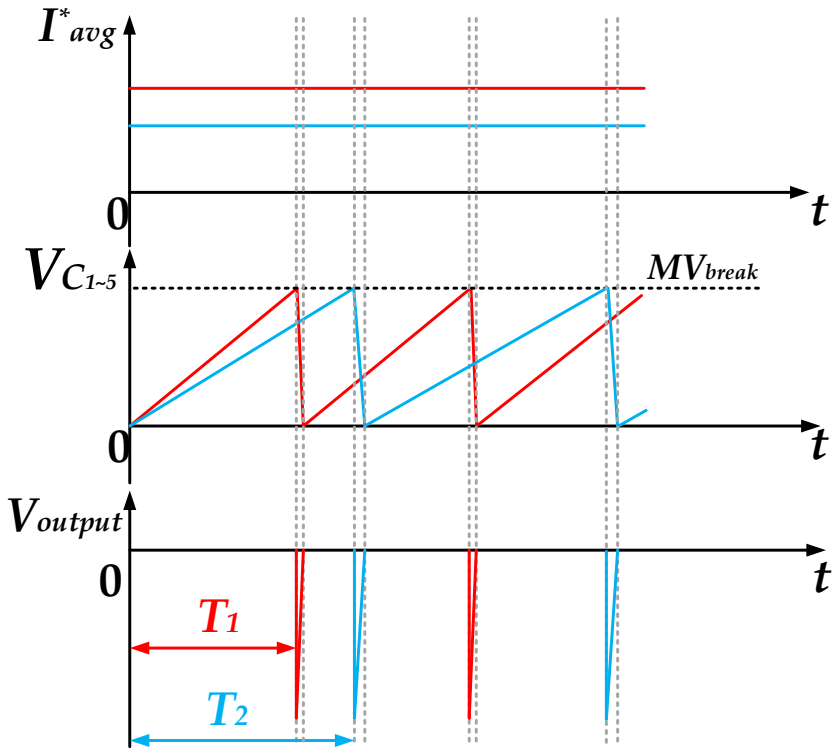

Figure 4. The theoretical waveforms with different average currents in the novel generator.

To further improve the energy efficiency of the generator, isolation inductors are used to replace the isolation resistors, as shown in Figure 5.

The inductors store or release the energy as current changes, and the energy loss of the circuit can be reduced. At the same time, a BJT T16 is added to ensure the first stage of the circuit is turned on first. As shown in Figure 5, C1 is charged by the series-resonant charging power supply through R1 as shown in the red line, and the Base current I_b can turn on T16. The capacitors C1~C5 will be charged as indicated by the blue arrowed lines. Since C1 is charged first, T1~T3 will breakdown first as if they are turned on first. Then, the

other stages will rapidly break down due to the overvoltage, and the capacitors discharge to the load in series.

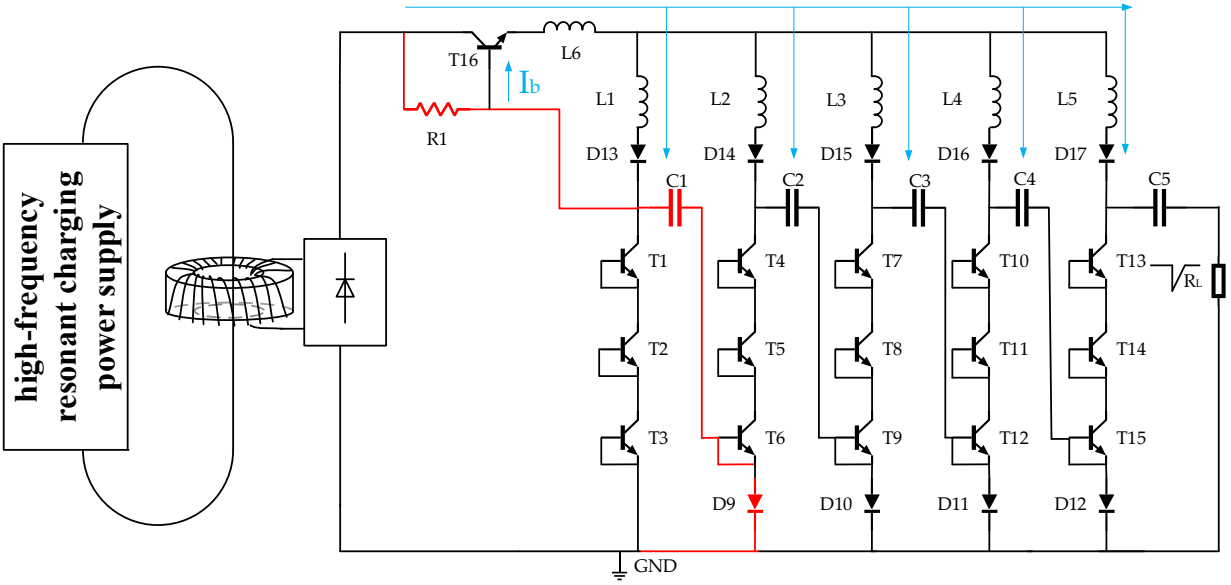

Figure 5. The nanosecond pulse generator using isolating inductors (circuit II).

3. Energy Efficiency Analysis of the Proposed Nanosecond Marx Generator

The energy loss can be divided into charging loss and discharging loss [16].

3.1. Charging Loss

The isolation resistors R_c consume energy whenever there is current flowing through them, as shown in Figure 2. The energy loss comes mainly from these isolation resistors. The energy loss during charging can be calculated as Equation (5).

$$P_{Rc} = \frac{N}{T}\int_0^T \left(R_c I'^2\right) dt \tag{5}$$

$$I' = \frac{|I(t)|}{N \cdot n} \tag{6}$$

where T is the charging time. N is the number of stages in the Marx generator and the number of storage capacitors. N is the turns ratio of the transformer. I' represents the branch current flowing through each storage capacitor C_N during the charging period.

The average current I_a is used to compare the energy W_{Rc} consumed by R_c and the energy W_c stored in capacitors C_N in the charging period. Ignore R_L (R_L<<R_c), at this time, I_a represents the average charging current on each energy storage capacitor C_N.

$$I_a = \frac{I^*_{avg}}{N} = C\frac{du_c}{dt} \tag{7}$$

W_{Rc} and W_c can be calculated by Equations (8) and (9). When T > 2R_cC, W_c will be higher than W_{Rc}, and the charging energy efficiency of the storage capacitor will be higher than 50%. In this case, the charging efficiency is greater than that of the DC source. However, many practical problems were not considered, so the specific situation needs further experimental exploration.

$$W_{Rc} = NI_a^2 R_c T \tag{8}$$

$$W_c = \frac{1}{2}Ncu_c^2 = \frac{NI_a^2 T^2}{2C} \tag{9}$$

3.2. Discharging Loss

During the discharging period, as indicated by the red arrowed line in Figure 6, the energy loss comes from the avalanche BJTs and the isolation resistors. After the avalanche BJTs are turned on, all the storage capacitors are discharged to the load resistor R_L. The avalanche BJT can be equivalent to a small resistor r_o. The instantaneous current i_L in the discharge circuit can be expressed by Equation (10) in the case of all the avalanche BJTs being turned on.

$$i_L = \frac{V_{peak}}{R_L} e^{-t/\tau} \tag{10}$$

where

$$\tau = (N_T r_o + R_L)C/N \tag{11}$$

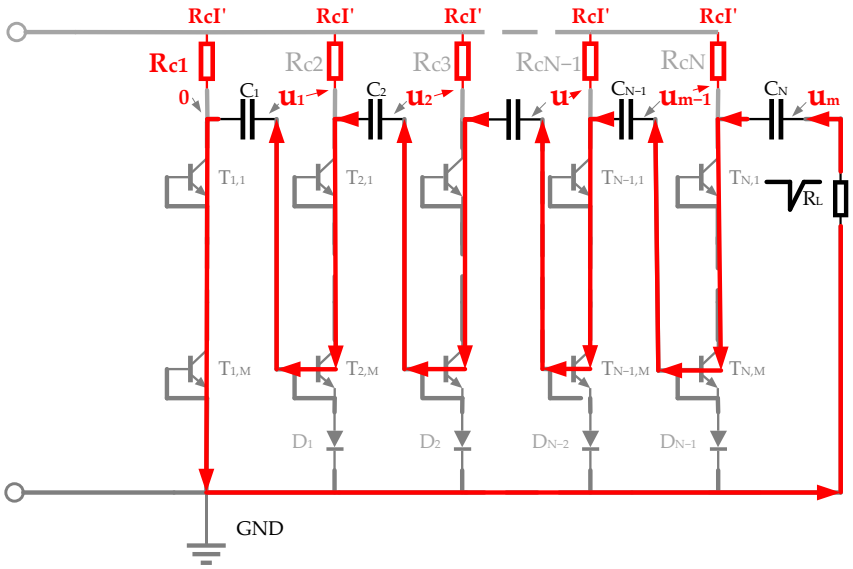

Figure 6. Schematic diagram of isolation resistance R_c loss in the discharge period.

V_{peak} is the peak voltage of the output pulses, τ is the time constant of the discharge circuit expressed by Equation (11), and N_T is the number of avalanche transistors.

The potential at the right end of the "mth" capacitor is shown in Equation (12), where u_1~u_m are shown in Figure 6.

$$u_m = \frac{-m}{N_c} V_{peak} e^{-t/\tau} \tag{12}$$

Take Rc_1 as an example. As shown in Figure 6, at the beginning of discharge, the potentials at two pins of Rc_1 are R_cI' and 0, respectively. Because the discharge duration is very short, R_cI' can be considered as a constant. The discharge loss on resistance R_1 can be expressed by Equation (13).

$$P_{Rc1} = f \int_0^A \frac{(R_cI' - 0)^2}{R_1} dt \tag{13}$$

where A is the turn-on time of the BJTs, f is the discharging frequency, which is also the pulse repetition frequency.

The energy consumed by the isolation resistors is shown in Equation (14). In this case, the influence of r_o on u_m can be ignored.

$$P_{Rdischarge} = f \int_0^A \sum_{m=0}^{N-1} \frac{(R_cI' - u_m)^2}{R_c} dt \tag{14}$$

The power consumed on the avalanche BJTs is shown in Equation (15).

$$P_{\mathrm{T}} = fN \int_0^A \mathrm{i}_L^2 r_{\mathrm{o}} dt \tag{15}$$

3.3. Efficiency Analysis

To analyze the energy efficiency of the circuit more intuitively, the charging efficiency η_{c} and discharge efficiency η of the circuit can be calculated by Equation (16).

$$\eta_{\mathrm{c}} = \frac{P_{\mathrm{c}}}{P_{\mathrm{in}}} \times 100\%, \ \eta = \frac{P_{\mathrm{o}}}{P_{\mathrm{in}}} \times 100\% \tag{16}$$

$$P_{\mathrm{c}} = \frac{1}{2} f N C u_{\mathrm{c}}^2 \tag{17}$$

$$P_{\mathrm{o}} = f \int_0^T U_{\mathrm{o}}^2 / R_{\mathrm{L}} dt \tag{18}$$

$$P_{\mathrm{in}} = f V_{\mathrm{dc}} \int_0^T i dt \tag{19}$$

where P_{c} is the power of the storage capacitors expressed by Equation (17), P_{o} is the output power of the generator, P_{in} is the input power as shown by Equations (18) and (19).

Because the output waveform of the generator can be regarded as a zero-order Gaussian waveform, and the normalized zero-order Gaussian function can be expressed by Equation (20) [17,18]. Then, Equation (21) can be obtained from Equations (18) and (20).

$$f_0(\mathrm{t}) = U_{\mathrm{e}} \exp\left(-\alpha_0 t^2\right), \ \alpha_0 = \frac{4 \ln 2}{T_{\mathrm{e}}^2} \tag{20}$$

$$P_{\mathrm{o}} = f_{\mathrm{e}} \int_{-\infty}^{\infty} \left[\frac{U_{\mathrm{e}}^2}{R_{\mathrm{L}}} \exp\left(-2 \cdot \frac{4 \ln(2)}{T_{\mathrm{e}}^2} t^2 \right) \right] dt = \frac{\sqrt{\pi}}{2\sqrt{2 \ln(2)}} \frac{T_{\mathrm{e}} f_{\mathrm{e}} U_{\mathrm{e}}^2}{R_{\mathrm{L}}} \tag{21}$$

where U_{e} is the amplitude of the output voltage and T_{e} is the full-width at half-maximum (FWHM) of the output voltage. F_{e} represents the repeatable frequency of the circuit and R_{L} is the load resistance.

4. Experiments

To verify the energy efficiency of the novel generator, a 3 × 5-stage Marx generator based on the avalanche BJTs (circuit I) is built, as shown in Figure 7. It mainly consists of an FPGA controller, a full-bridge circuit, a rectifying circuit, and a 3 × 5-stage Marx generator. The DC source is a Hanshenpuyuan-5000 (HS-5000). The input voltage and power can be read directly from the DC source. The switches of the full-bridge circuit are IXYX120N120C3, the resonant inductor L_{r} is about 5 μH, the resonant capacitor C_{r} is about 1.5 μF, the turns ratio of the booster transformer TX is about 60, the model of the diodes from D1 to D12 is DSEP12-12A, the BJTs are C1815GR, the energy-storage capacitors are 1nF ceramic capacitors, the isolation resistors R_{C} are 5 kΩ cement resistors, and the load resistor R_{L} is 50 Ω.

Because of series resonant charging, the voltage of the storage capacitors will increase until the avalanche voltage is reached. When the voltage is higher than the breakdown voltage of the Collector and Emitter, the avalanche BJTs will automatically turn on. When V_{dc} is 40 V, and f_{s} is 25 kHz, the voltage waveform of the load is shown in Figure 8. The nanosecond output pulses with a repetitive frequency of 50 kHz, a pulse FWHM width of 12.68 ns, and an amplitude of 2.9 kV are obtained over a resistive load. According to Equation (21), P_{o} is about 80.27 W.

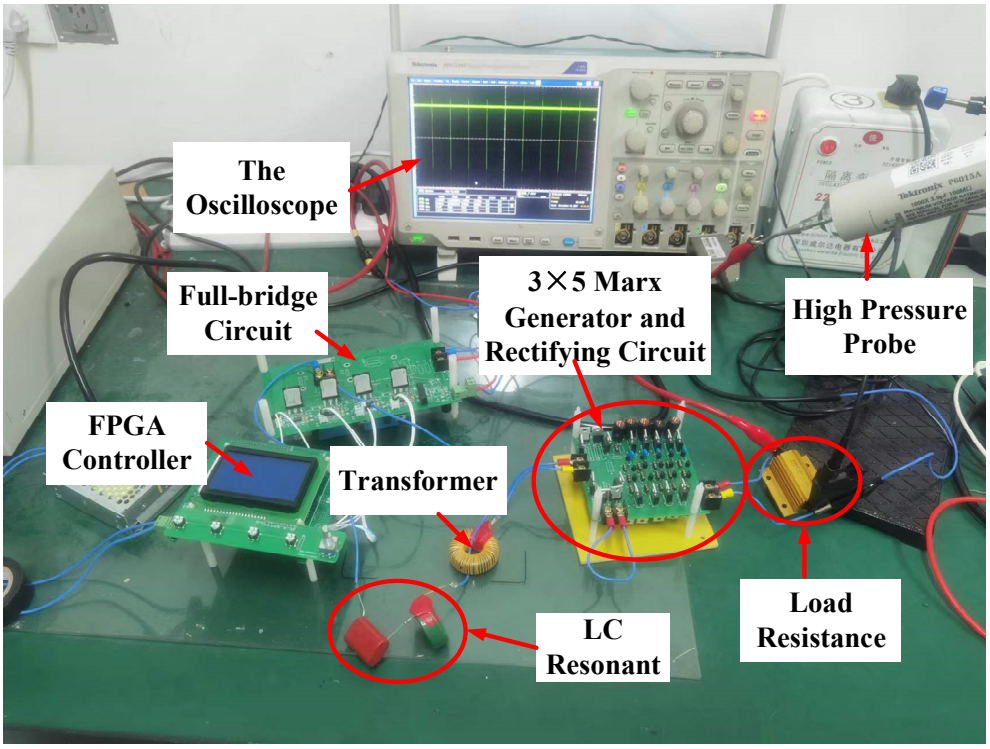

Figure 7. A photograph of the 3 × 5 stage Marx generator based on the avalanche BJTs.

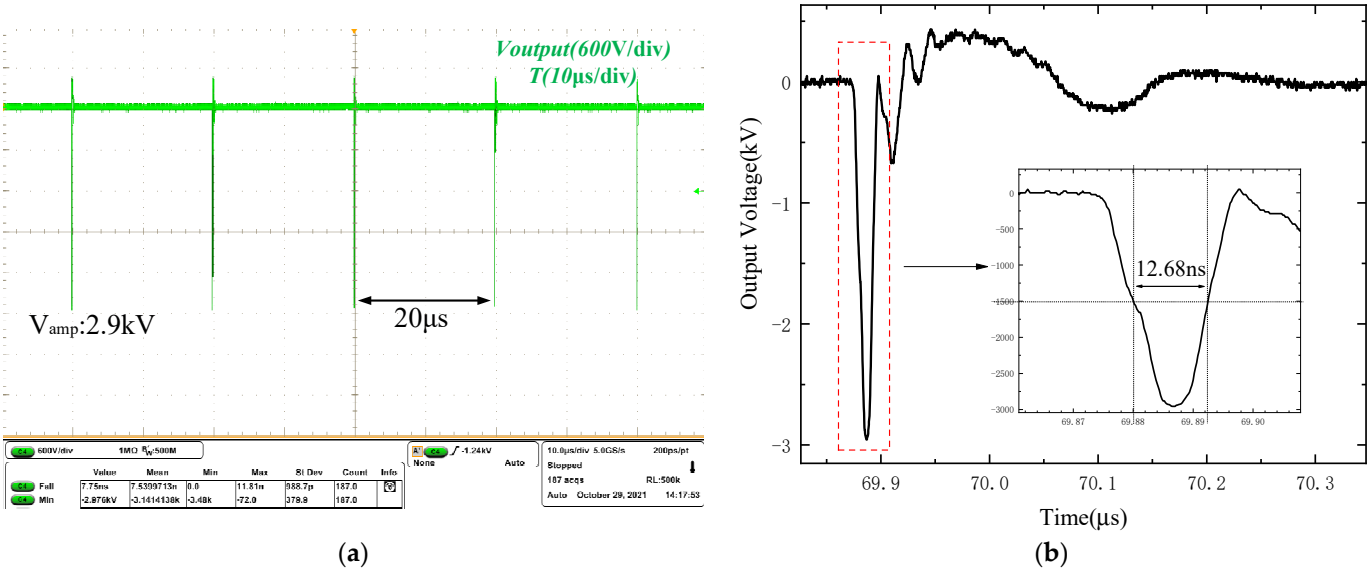

Figure 8. The voltage waveform of the load (circuit I): (**a**) discharge waveform with a repeatable frequency of 50 kHz; (**b**) enlarged view of load voltage.

The voltage waveform of the energy-storage capacitors and the waveform of the resonant current i_r are shown in Figure 9. It can be seen that a resonant current charges the capacitors in the circuit. When the resonant current is zero, the voltage of the capacitors remains unchanged. The peak voltage of the capacitors is about 750 V in a charging period (V_{dc} is 40 V, n is about 60, and the theoretical maximum voltage of $C_{1\sim5}$ is about 2400 V). However, due to the series BJTs, when the capacitor voltage is about 750 V, the Marx generator will enter the discharge period. At this time, the avalanche breakdown voltage of the three BJT connected in series is about 750 V which is much lower than 2400 V, the series-resonant power supply will always charge the capacitors with a constant average current. According to Equation (17), P_c is about 70.31 W. The power stored in the capacitors

is even lower than the power of the load 80.27 W, because the series-resonant power supply still operates during the discharge period and releases energy to the resistive load, which further improves the energy efficiency. The input power can be read from the parameters of HS-5000 (here, P_{in} is about 105.04 W). According to Equation (16), η_c is calculated to be 66.94% and η is 76.42%.

The improved nanosecond Marx generator using isolating inductors build the circuit as shown in Figure 5. When V_{dc} is 40 V, and f_s is 25 kHz, the voltage waveform of the load is shown in Figure 10. The nanosecond output pulses with a repetitive frequency of 50 kHz (as shown in Figure 10a), a pulse width of 8.45 ns, and an amplitude of 4.0 kV are obtained on a resistive load. According to Equation (21), P_o is about 101.81 W. Moreover, the discharge frequency f can be continuously adjusted in a particular range by changing the switching frequency f_s. The discharge voltage on the load is very stable and will not be affected by the switching frequency, as shown in Figure 10b.

The voltage waveform of the energy storage capacitors and the waveform of the resonant current i_r are shown in Figure 11. The maximum voltage of the capacitors is about 850 V in a charging period. According to Equation (17), P_c is about 90.31 W. The voltage of capacitors in circuit II is higher than that in circuit I because of the boost effect of the inductors. As shown in Figure 11, when the capacitors discharge to the load in series, the charging current decreases. These charging currents in the isolating inductors also flow into the resistive load and the capacitors. Therefore, the voltage in capacitors increases and the energy efficiency also increases. The input power is about 108.03 W. η_c and η are calculated as 83.60%, 94.24% according to Equation (16). Compared with circuit I, the capacitor charging efficiency and energy efficiency of circuit II are increased by 24.89% and 23.32%, respectively. The calculation formula is shown in Equation (22).

$$\eta_{increase} = \frac{\eta_{II} - \eta_I}{\eta_I} \times 100\%. \quad (22)$$

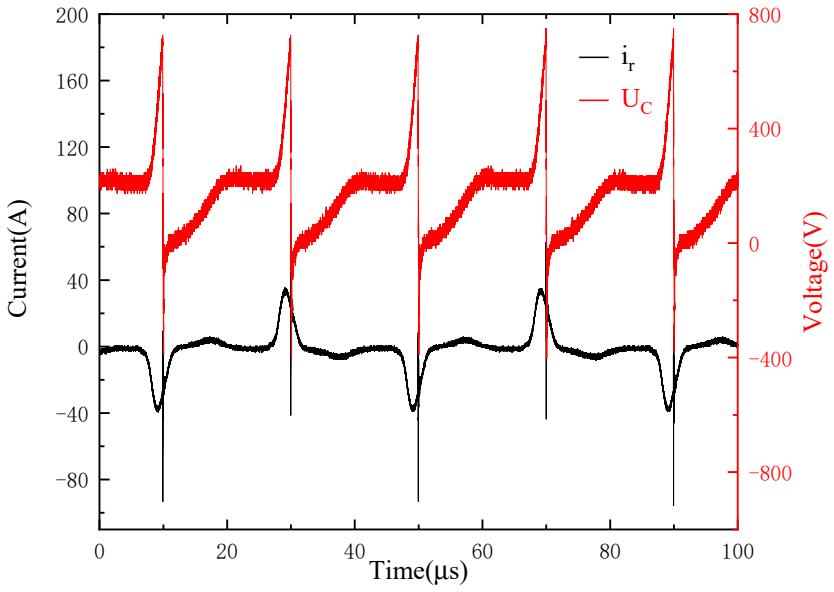

Figure 9. The waveform of the voltage on the energy-storage capacitors U_c and the resonant current i_r (circuit I).

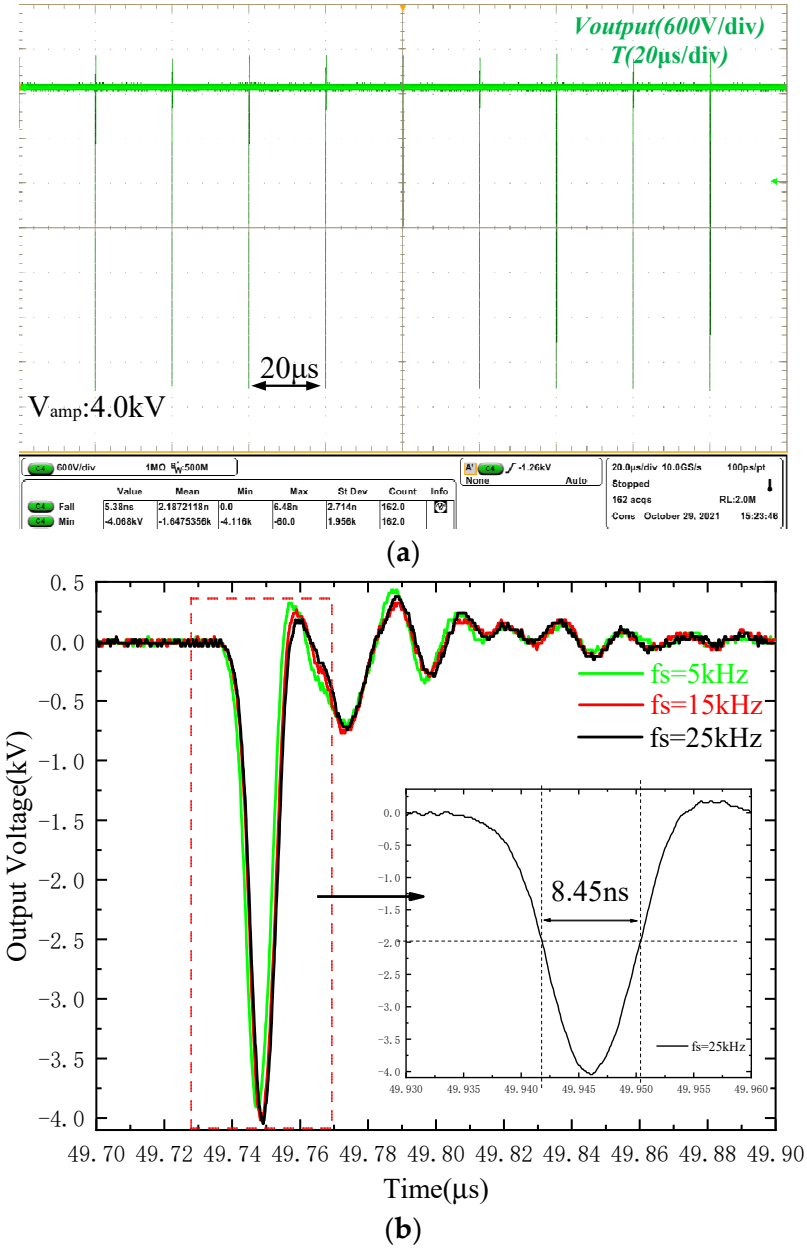

Figure 10. The voltage waveform of the load (circuit II): (**a**) discharge waveform with a repeatable frequency of 50 kHz; (**b**) enlarged view of load voltage in a different frequency.

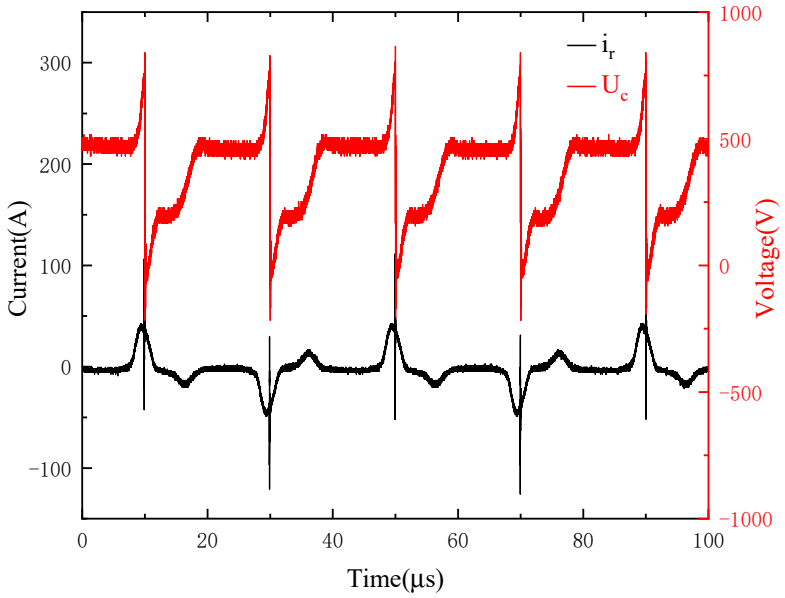

Figure 11. The waveform of the energy-storage capacitors U_c and the resonant current i_r (circuit II).

5. Discussion

As shown in Table 1, compared with the energy efficiency below 30% in the generators in references [6,8], the energy efficiency of the proposed nanosecond Marx generator in this paper is greatly improved to 76% and 94%.

Table 1. Efficiency comparison of nanosecond Marx generators based on avalanche BJTs.

	Reference [6]	Reference [8]	Circuit I	Circuit II
η/%	21.55	26.67	76.42	94.24
η_c/%	52.38	61.52	66.94	83.60

Reference [6], a traditional nanosecond pulse generator with avalanche BJTs charged by a DC source. Reference [8], an improved Marx generator with avalanche BJTs using an isolation BJT.

As shown in Figure 12, considering the effect of switching frequency on discharge frequency and amplitude of the pulse, the discharge frequency can be adjusted continuously from 10 to 60 kHz. When the discharge frequency is below 50 kHz, the output voltage amplitude U_m is about 4 kV. The voltage amplitude declines when the discharge frequency is higher than 50 kHz, as shown by the red line in Figure 12 demonstrating the effect of switching frequency on discharge frequency and amplitude of the pulse. With the increase in discharging frequency, the generator's input power and output power increase, as shown in Figure 13. When the frequency is greater than 50 kHz, the input power reaches the maximum power of HS-5000, and the pulse amplitude will decrease as the discharge frequency of the generator continues to increase to maintain the output power. The energy efficiency of the generator remains very high with different discharging frequencies as shown in Figure 14. The comparison of theoretical and practical energy efficiency values is very close, and the error rate is less than 5%, which verifies the reliability of the calculation. According to the analysis above, the maximum energy efficiency of the generator is 94.24%.

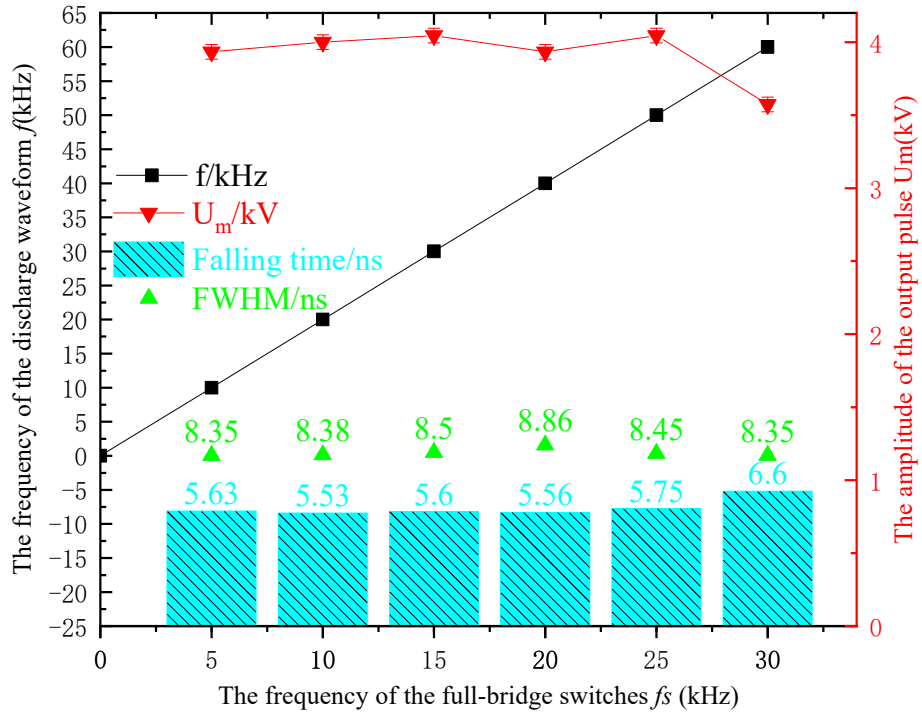

Figure 12. The effect of switching frequency on discharge frequency and amplitude of the pulse.

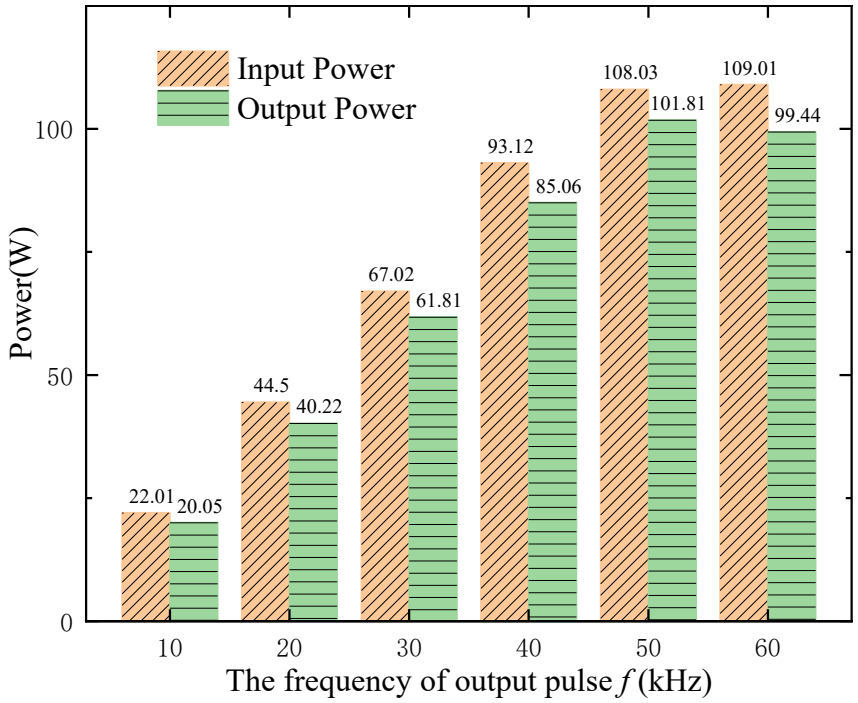

Figure 13. The power with a different output pulse frequency.

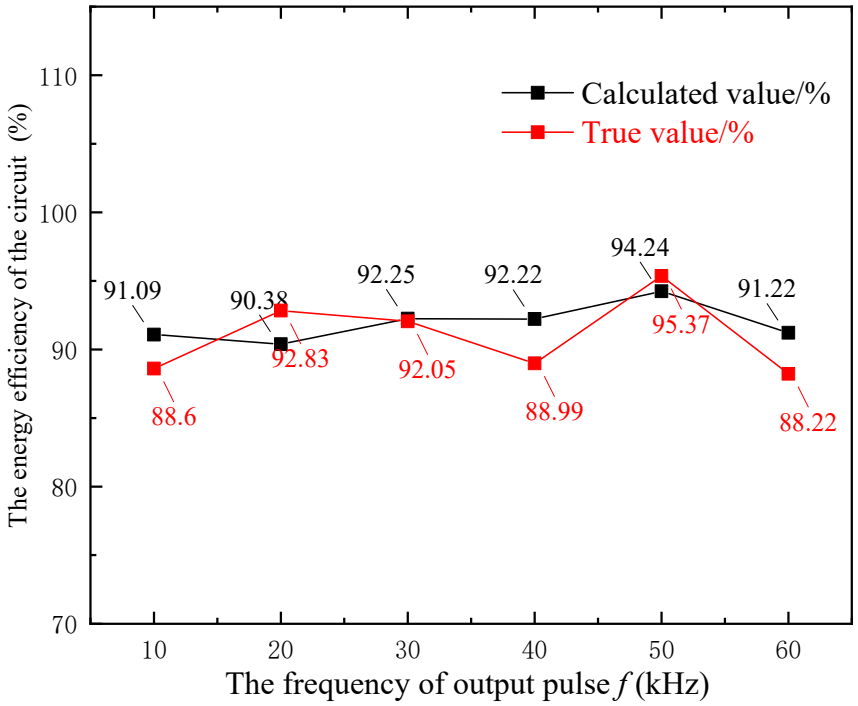

Figure 14. The energy efficiency of the circuit at different output pulse frequencies.

In fact, in addition to the energy efficiency used in this paper, some researchers also use voltage efficiency η_{voltage} to compare the performance between circuits, as shown in References [19,20]. The equation of voltage efficiency is shown in Equation (23). The key parameters are summarized in Table 2. The new generator proposed in this paper significantly improves the voltage efficiency of the circuit from 50% to 90%. Compared with the traditional structure, the number of BJTs required to achieve the 4 kV repetition output is significantly reduced to 16. In addition to substantially improving voltage efficiency, the proposed generator in this paper also achieves a high repetition frequency which is adjustable from 10 to 60 kHz.

$$\eta_{\text{voltage}} = \frac{V_{\text{peak}}}{N_{\text{c}} \cdot u_{\text{c}}} \times 100\% \tag{23}$$

where V_{peak} is the peak voltage of the output pulses, N_{c} is the number of energy storage capacitors, and u_{c} is the voltage of the energy-storage capacitors.

Table 2. Parameter comparison of nanosecond Marx generators based on avalanche BJTs.

	Reference [10]	Reference [19]	Reference [20]	Reference [21]	Circuit I	Circuit II
Amplitude/kV	4.0	6.5	4.0	3.9	2.9	4.0
Front edge time/ns	6	3.65	0.24	0.3	7.7	5.7
Pulse width/ns	20	/	5.2	1.8	12.68	8.45
Repetition frequency/kHz	2	1	0.01	30	10~60	10~60
Number of transistors	36	60	24	80	15	16
Load/Ω	50	75	50	50	50	50
Voltage efficiency/%	37	56.5	55.6	16.3	77.33	94.12

6. Conclusions

A novel nanosecond Marx generator based on avalanche BJTs is proposed in this paper. No triggering signal is required since avalanche BJTs breakdown automatically as long as the Collector-Emitter voltage over BJTs exceeds the breakdown voltage. The frequency

of the output pulses can be adjusted by controlling the average charging current of the full-bridge circuit. The output voltage can be increased by connecting more avalanche BJTs in series or increasing the number of stages in this nanosecond Marx generator. A full-bridge series-resonant charging power supply is used to charge the energy stored capacitors instead of the DC voltage source, which considerably improves the energy efficiency. Replacing the resistors with isolation inductors can further improve efficiency. A 3×5-stage nanosecond Marx generator was built, and the nanosecond output pulses with a pulse width of 12.68 ns, a voltage amplitude of 2.9 kV, and a repetitive frequency 50 kHz were obtained over a 50 Ω load. The charging energy efficiency of the capacitor η_c and the energy efficiency of the circuit η improved to 66.94% and 76.42%, respectively. When isolation inductors are used to replace the resistors, the peak voltage of the output pulses increased to 4 kV, and the energy efficiency η was increased to 94%. From the results, the frequency of the output pulses is adjustable from 10 to 60 kHz.

Author Contributions: Data curation, Yuan Chai; Funding acquisition, J.R.; Investigation, Y.C.; Methodology, Z.L.; Validation, S.J.; Writing—original draft, Z.L.; Writing—review & editing, J.R. All authors have read and agreed to the published version of the manuscript.

Funding: This research was funded by [Ministry of Science and Technology: National Key R&D Program of China] grant number [2019YFC0119102]. The APC was funded by [MDPI].

Conflicts of Interest: The authors declare no conflict of interest.

References

1. Krishnaswamy, P.; Kuthi, A.; Vernier, P.T.; Gundersen, M.A. Compact Subnanosecond Pulse Generator Using Avalanche Transistors for Cell Electroperturbation Studies. *IEEE Trans. Dielectr. Electr. Insul.* **2007**, *14*, 873–877. [CrossRef]
2. Bishop, A.I.; Barker, P.F. Subnanosecond pockels cell switching using avalanche transistors. *Rev. Sci. Instrum.* **2006**, *77*, 3066. [CrossRef]
3. Jiang, Z.; Zhang, S.; Liao, X.; Wang, W.; Liu, D.; Ding, T. Progress in the application of non-thermal plasma in degradation and modification of biopolymers. *Food Sci.* **2017**, *38*, 282–288.
4. Gao, M.X.; Xie, Y.-Z.; Li, K.-J.; Qiu, Y.-X.; Wang, S.-F.; Wang, S.-Q.; Hu, Y.-H.; Du, Z.-W. Traveling-Wave Marx Circuit for Generating Repetitive Sub-Nanosecond Pulses. *IEEE Trans. Electromagn. Compat.* **2019**, *61*, 1271–1279. [CrossRef]
5. Shen, S.; Yan, J.; Wang, Y.; Sun, G.; Ding, W. Further Investigations on a Modified Avalanche Transistor-Based Marx Bank Circuit. *IEEE Trans. Instrum. Meas.* **2020**, *69*, 8506–8513. [CrossRef]
6. Li, Z.; Li, P.; Rao, J.; Jiang, S.; Sakugawa, T. Theoretical Analysis and Improvement on Pulse Generator Using BJTs as Switches. *IEEE Trans. Plasma Sci.* **2016**, *44*, 2053–2059. [CrossRef]
7. He, R.; Li, Y.; Liu, Z.; Jin, J.; Sun, Z. Development of a High Peak Voltage Picoseconds Avalanche BJT Based Marx Bank Circuit. *IEEE Access* **2021**, *9*, 64844–64851. [CrossRef]
8. Rao, J.; Pi, T.; Zi, L.; Song, J. Design on High-frequency Nanosecond Pulse Power Source with Truncated Switches. *High Volt. Eng.* **2017**, *43*, 1800–1807.
9. Rao, J.; Zhang, W.; Jiang, S.; Li, Z. Nanosecond pulse generator based on cascaded avalanche BJTs and Marx circuits. *IEEE Trans. Dielectr. Electr. Insul.* **2019**, *26*, 374–380. [CrossRef]
10. Yan, J.; Shen, S.; Ding, W. High-Power Nanosecond Pulse Generators with Improved Reliability by Adopting Auxiliary Triggering Topology. *IEEE Trans. Power Electron.* **2020**, *35*, 1353–1364. [CrossRef]
11. Lippincott, A.C.; Nelms, R.M. A capacitor-charging power supply using a series-resonant topology, constant on-time/variable frequency control, and zero-current switching. *IEEE Trans. Ind. Electron.* **1991**, *38*, 438–447. [CrossRef]
12. Nelms, R.M.; Schatz, J.E. A capacitor charging power supply utilizing a Ward converter. *IEEE Trans. Ind. Electron.* **1992**, *39*, 421–428. [CrossRef]
13. Su, J.; Wang, L.; Ding, Y.; Song, X. Analysis and design of series resonant charging power supply. *High Power Laser Part. Beams* **2004**, *16*, 1611–1614.
14. Zhong, H.; Xu, Z.; Zou, X.; Zou, Y.; Yang, L.; Chao, Z. Current characteristic of high voltage capacitor charging power supply using a series resonant topology. In Proceedings of the IECON'03 29th Annual Conference of the IEEE Industrial Electronics Society (IEEE Cat. No.03CH37468), Roanoke, VA, USA, 2–6 November 2003; pp. 373–377.
15. Lin, L.; Zhong, H.; Deng, Y.; Gao, L.; Luo, X.; Li, A.; Liao, Y. Analysis and design of voltage maintaining method for series resonant capacitor charging power supply. In Proceedings of the 2014 IEEE Applied Power Electronics Conference and Exposition–APEC 2014, Worth, TX, USA, 16–20 March 2014; pp. 3249–3254.
16. Li, P. Research on Pulsed Power Generator Using Avalanche BJTs as Switches. Master's Thesis, The University of Shanghai For Science & Technology, Shanghai, China, 2016.

17. Zhang, H. Electromagnetic Radiation and Suppression Based on Marx Circuit of Avalanche BJT. Master's Thesis, University of Electronic Science and Technology of China, Chengdu, China, 2020.
18. Zhang, M. Development of Sub-nanosecond Pulse Source Based on Marx Circuit. Master's Thesis, University of Electronic Science and Technology of China, Chengdu, China, 2020.
19. Cheng, L.; Chen, Z.; Wang, H.; Guo, F.; Wu, G.; Xie, L.; Xiao, J.; Wang, Y.; Shen, S.; Ding, W. A Novel Avalanche Transistor-Based Nanosecond Pulse Generator with a Wide Working Range and High Reliability. *IEEE Trans. Instrum. Meas.* **2021**, *70*, 1–14. [CrossRef]
20. Yan, J.; Shen, S.; Wang, Y.; Zhang, S.; Cheng, L.; Ding, W. A novel trigger for pseudospark switch with high repetition rate, low jitter, and compact structure. *Rev. Sci. Instrum.* **2018**, *89*, 065102. [CrossRef] [PubMed]
21. Heeren, T.; Ueno, T.; Wang, D.; Namihira, T.; Katsuki, S.; Akiyama, H. Novel dual Marx Generator for microplasma applications. *IEEE Trans. Plasma Sci.* **2005**, *33*, 1205–1209. [CrossRef]